Performance of prototypes for the ALICE electromagnetic calorimeter

J. Allen,[5] T. Awes,[14] A. Badalá,[3] S. Baumgart*,[13] R. Bellwied,[4] L. Benhabib,[12] C. Bernard,[7] N. Bianchi,[5]
F. Blanco,[2, 8] Y. Bortoli,[12] G. Bourdaud,[12] O. Bourrion,[7] B. Boyer,[7] E. Bruna,[13] J. Butterworth,[15]
H. Caines,[13] D. Calvo Diaz Aldagalan,[19] G.P. Capitani,[5] Y. Carcagno,[7] A. Casanova Diaz,[5] M. Cherney,[15]
G. Conesa Balbastre,[5] T.M. Cormier,[4] L. Cunqueiro Mendez,[5] H. Delagrange,[12] M. Del Franco,[5] M. Dialinas,[12]
P. Di Nezza,[5] A. Donoghue,[17] M. Elnimr,[4] A. Enokizono,[14] M. Estienne,[12] J. Faivre,[7] A. Fantoni,[5] F. Fichera,[3]
B. Foglio,[7] S. Fresneau,[12] J. Fujita,[15] C. Furget,[7] S. Gadrat,[7] I. Garishvili,[10] M. Germain,[12] N. Giudice,[2]
Y. Gorbunov,[15] A. Grimaldi,[3] N. Guardone,[2] R. Guernane,[7] C. Hadjidakis,[12] J. Hamblen,[10] J.W. Harris,[13]
D. Hasch,[5] M. Heinz,[13] P.T. Hille,[13] D. Hornback,[10] R. Ichou,[12] P. Jacobs,[1] S. Jangal,[18] K. Jayananda,[15]
J.L. Klay,[17] A.G. Knospe,[13] S. Kox,[7] J. Kral,[9] P. Laloux,[12] S. LaPointe,[4] P. La Rocca,[16, 2] S. Lewis,[17] Q. Li,[4]
F. Librizzi,[3] D. Madagodahettige Don,[8] I. Martashvili,[10] B. Mayes,[8] T. Milletto,[12] V. Muccifora,[5] H. Muller,[6]
J.F. Muraz,[7] C. Nattrass,[13, 10] F. Noto,[2] N. Novitzky,[9] G. Odyniec,[1] A. Orlandi,[5] A. Palmeri,[3] G.S. Pappalardo,[3]
A. Pavlinov,[4] W. Pesci,[5] V. Petrov,[4] C. Petta,[2] P. Pichot,[12] L. Pinsky,[8] M. Ploskon,[1] F. Pompei,[4] A. Pulvirenti,[2]
J. Putschke,[13] C.A. Pruneau,[4] J. Rak,[9] J. Rasson,[1] K.F. Read,[10] J.S. Real,[7] A.R. Reolon,[5] F. Riggi,[2] J. Riso,[4]
F. Ronchetti,[5] C. Roy,[18] D. Roy,[12] M. Salemi,[3] S. Salur,[1] M. Sharma,[4] D. Silvermyr,[14] N. Smirnov,[13] R. Soltz,[11]
V. Sparti,[3] J.-S. Stutzmann,[12] T.J.M. Symons,[1] A. Tarazona Martinez,[20] L. Tarini,[4] R. Thomen,[15] A. Timmins,[4]
M. van Leeuwen†,[1] R. Vieira,[5] A. Viticchié,[5] S. Voloshin,[4] D. Wang,[21] Y. Wang,[21] and R.M. Ward[17]

[1]*Lawrence Berkeley National Laboratory, Berkeley 94720, United States*
[2]*Dipartimento di Fisica e Astronomia dell'Università Catania e Sezione INFN, 95123 Catania, Italy*
[3]*Sezione INFN, 95123 Catania, Italy*
[4]*Wayne State University, Detroit 48202, United States*
[5]*Laboratori Nazionali di Frascati, INFN, 00044 Frascati, Italy*
[6]*CERN, European Organization for Nuclear Research, 1211 Geneva, Switzerland*
[7]*LPSC, Université Joseph Fourier Grenoble 1, CNRS/IN2P3/INPG,
Institut Polytechnique de Grenoble, 38026 Grenoble Cedex, France*
[8]*University of Houston, Houston 77204, United States*
[9]*Helsinki Institute of Physics (HIP) and University of Jyväskylä, 40351 Jyväskylä, Finland*
[10]*University of Tennessee, Knoxville 37996, United States*
[11]*Lawrence Livermore National Laboratory, Livermore 94550, United States*
[12]*SUBATECH, Ecole des Mines de Nantes, Université de Nantes, CNRS-IN2P3, 44307 Nantes, Cedex 3, France*
[13]*Yale University, New Haven 06511, United States*
[14]*Oak Ridge National Laboratory, Oak Ridge 37831, United States*
[15]*Creighton University, Omaha Nebraska 68178, United States*
[16]*Museo Storico della Fisica e Centro Studi e Ricerche Enrico Fermi, 00184 Roma, Italy*
[17]*California Polytechnic State University, San Luis Obispo 93407, United States*
[18]*IPHC, Institute Pluridisciplinaire Hubert Curien, Université Louis Pasteur, CNRS-IN2P3, 67037 Strasbourg, Cedex 2, France*
[19]*University of Valencia, 46010 Valencia, Spain*
[20]*Valencia Polytechnic University, 46022 Valencia, Spain*
[21]*Hua–Zhong Normal University, 430079 Wuhan, China*
(Dated: December 10, 2009)

The performance of prototypes for the ALICE electromagnetic sampling calorimeter has been studied in test beam measurements at FNAL and CERN. A 4×4 array of final design modules showed an energy resolution of about $11\% / \sqrt{E(\text{GeV})} \oplus 1.7\,\%$ with a uniformity of the response to electrons of 1% and a good linearity in the energy range from 10 to 100 GeV. The electromagnetic shower position resolution was found to be described by 1.5 mm $\oplus$ 5.3 mm $/\sqrt{E(\text{GeV})}$. For an electron identification efficiency of 90% a hadron rejection factor of > 600 was obtained.

INTRODUCTION

*now at: RIKEN, The Institute of Physical and Chemical Research, Wako 351-0198, Japan
†now at: Universiteit Utrecht, 3508 Utrecht, Netherlands

ALICE (A Large Ion Collider Experiment) at the LHC is designed to carry out comprehensive measurements of high energy nucleus–nucleus collisions, in order to study QCD matter under extreme conditions and to explore the phase transition between confined matter and the

Quark-Gluon Plasma (QGP) [1, 2].

ALICE contains a wide array of detector systems for measuring hadrons, leptons and photons. The ALICE detector is described in detail in [3]. The large acceptance Electromagnetic Calorimeter (EMCal), which is foreseen to be fully installed in 2011, significantly enhances ALICE's capabilities for jet measurements. The ALICE EMCal is designed to provide the following functions:

– efficient and unbiased fast level L0 and L1 trigger on high energy jets

– measurement of the neutral portion of jet energy

– improvement of jet energy resolution

– measurement of high momentum photons, π^0 and electrons

– γ / π^0 discrimination up to 30 GeV [1]

– e / h separation (for momenta larger than 10 GeV/c)

– high uniformity of response for isolated electromagnetic clusters.

From Monte Carlo simulations, a detector energy resolution of the order of about $15\%/\sqrt{E(\text{GeV})} \oplus 2\%$ was found to be sufficient for the jet physics program and is fixed as the minimum detector requirement. The electron and photon physics programs, however, would benefit from better resolution.

The overall design of the EMCal is heavily influenced by its integration within the ALICE [3] setup which constrains the detector acceptance to a region of about 110 degrees in azimuth ϕ, $-0.7 < \eta < 0.7$ in pseudo-rapidity and 4.35 m < R_{EMCal} < 4.7 m radial distance .

This paper presents the performance of prototype modules studied in test beam measurements at FNAL and at CERN. The goals of these measurements were the determination of the intrinsic energy and position resolution, the investigation of the linearity and uniformity of the detector response, the determination of the light yield per unit of energy deposit and a study of the response to electrons and hadrons. Furthermore, monitoring and calibration tools were successfully implemented and tested.

CALORIMETER MODULE DESIGN AND READOUT

The chosen technology is a layered Lead(Pb)-Scintillator(Scint) sampling calorimeter with wavelength shifting (WLS) fibers that run longitudinally through the Pb/Scint stack providing light collection (Shashlik) [4]. The basic building block is a module consisting of 2 × 2 optically isolated towers which are read out individually;

---

[1] Considering invariant mass and shower shape techniques only.

TABLE I: EMCal module physical parameters. Here, RL stands for Radiation Length and MR for the Moliere Radius.

Parameter	Value
Tower Size (at η=0)	~6.0 × ~6.0 × 24.6 cm^3
Tower Size	$\Delta\phi \times \Delta\eta = 0.0143 \times 0.0143$
Sampling Ratio	1.44 mm Pb / 1.76 mm Scint.
Layers	77
Scintillator	Polystyrene (BASF143E + 1.5%pTP + 0.04%POPOP)
Absorber	natural Lead
Effective RL X_0	12.3 mm
Effective MR R_M	3.20 cm
Effective Density	5.68 g/cm^3
Sampling Fraction	1/10.5
Radiation Length	20.1

each spans $\Delta\eta \times \Delta\phi = 0.014 \times 0.014$ each. White, acid free, bond paper serves as a diffuse reflector on the scintillator surfaces and provides friction between layers. The scintillator edges are treated with TiO_2 loaded reflector to improve the transverse optical uniformity within a single tower and to provide tower to tower optical isolation better than 99%.

The energy resolution for a sampling electromagnetic calorimeter varies with the sampling frequency approximately as $\sqrt{d_{\text{Sc}}/f_{\text{s}}}$, where d_{Sc} is the scintillator thickness in mm and f_{s} is the sampling fraction for minimum ionizing particles (MIPs). For optimum resolution in a given physical space and total radiation length, there is thus a desire to have the highest possible sampling frequency. Practical considerations, including the cost of the total assembly labour, suggest reducing the total number of Pb/Scint layers thus decreasing the sampling frequency. The requirement of a compact detector consistent with the EMCal integration volume and the chosen detector thickness of about 20 radiation lengths, results in a lead to scintillator ratio by volume of about 1:1.22 corresponding to a sampling geometry of Pb(1.44 mm)/Scint(1.76 mm).

The physical characteristics of the EMCal modules are summarized in Table I.

Scintillation photons produced in each tower are captured by an array of 36 Kuraray Y-11 (200 M), double clad, wavelength shifting (WLS) fibers. Each fiber within a given tower terminates in an aluminized mirror at the front face of the module and is integrated into a polished, circular group of 36 fibers at the photo sensor end at the back of the module. The 6.8 mm diameter fiber bundle from a given tower connects to the Avalanche Photodiode (APD) through a short light guide/diffuser. The selected photo sensor is the Hamamatsu S8664-55 avalanche photodiode chosen for operation in the high field inside the ALICE magnet. The APDs are operated at moderate gain for low noise and high gain stability in order to maximize energy and timing resolution. The

number of primary electrons generated in the APD by an electromagnetic shower is ≈ 4.4 electrons/MeV. The reverse bias voltage of the APDs are individually controlled to provide an electron multiplication factor (M) of 30 resulting in a charge output of ≈ 132 electrons/MeV from the APDs. All APDs used for the test beam measurements were previously calibrated [5]. The charge output from the APD is integrated by a Charge Sensitive Preamplifier (CSP) with a short rise time of ≈ 10 ns and a long decay time of ≈ 130 μs, i.e., approximately a step pulse. The amplitude of the step pulse is proportional to the number of integrated electrons from the APD and therefore proportional to the energy of the incident particle. The output from the CSP is conditioned with a second order gaussian shaper in order to make the signal suitable for digitization with the Alice TPC Readout Chip [6].

The readout electronics of the PHOS (PHoton Spectrometer) detector [7] of ALICE have been adopted for the EMCal front end electronics readout with only minor modifications, as the light yield per unit of energy deposit in the EMCal is similar to that of the PHOS [8]. A detailed description of the EMCal (PHOS) front end electronics (FEE) and their performance is given in Ref. [9]. The FEE has an effective 14-bit dynamic range over the interval 16 MeV to 250 GeV resulting in a Least Significant Bit on the low gain range of 250 MeV (10-bits) and on the high gain range of 16 MeV. Compared to PHOS, the coarse granularity of the EMCal yields higher occupancies. As the number of read out samples recorded is dictated by the total shaped pulse width, a shaping time of 200 ns (2 μs for PHOS) is chosen in order to keep the total data volume per central unit similar to PHOS and to fulfill the constraints from the total available bandwidth. This results in an electronic noise contribution of about 12 MeV per EMCal tower. However, due to the larger intrinsic energy resolution term of EMCal compared to PHOS the importance of the electronics noise contribution is much less. The effect of the shaping time on the calorimeter resolution has been studied in the test beam measurements performed at FNAL and is discussed in the next section.

TEST BEAM MEASUREMENTS

The performance of the first ALICE EMCal modules constructed according to final design was studied in CERN SPS and PS test beam lines in autumn 2007. The test utilized a stacked 4×4 array of EMCal modules (8×8 towers). All towers were instrumented with the full electronics chain with shapers and APD gains operated as planned in ALICE. A LED calibration system was installed in order to monitor time-dependent gain changes. The readout of the front end electronics used the standard ALICE data aquisition system.

Earlier test measurements were performed in November 2005 at the Meson Test Beam (MTEST) at FNAL utilizing a stacked 4×4 array of prototype EMCal modules (8×8 towers) of slightly different design than the final one, such as a radiation length of 22 X_0 and a sampling geometry of Pb(1.6 mm)/Scint(1.6 mm). For this test in particular, measurements were made for comparison of the performance with two different signal shaping times in the front end electronics. Two front end electronics cards (32 towers each) were used for the readout of the modules; one had the nominal 2 μs signal shaping time of the PHOS, and the other had a modified 200 ns shaping time as planned for EMCal.

The goals of the test beam measurements were:

- To determine the intrinsic energy and the position resolution using electron beams.

- To investigate the linearity and uniformity of the response; in particular across towers and module boundaries and for tilted or recessed modules.

- To determine the light yield (signal) per unit of deposited electromagnetic energy.

- To study the effect of shorter shaping times as planned for the final design.

- To study the energy dependence of the response to electrons and hadrons to determine the particle identification capabilities of the EMCal.

- To develop and investigate the performance of the monitoring and calibration tools (gain stability, time dependencies) using electron beams, MIPs from hadron beams, LED events and cosmic muons.

- To develop and test ALICE standard software for readout, calibration and analysis.

Test setup and beam line instrumentation

The characteristics of the test beams at FNAL and CERN are summarised in Table II.

TABLE II: Test beam parameters.

Lab	FNAL	CERN	CERN
test beam	MT6	SPS H6	PS T10
particle	e,h	e,h	e,h
intensity [s^{-1}]	10^3-10^4	10^2-10^3	10^2-10^3
$\Delta p/p$	$\pm$ 1%	$\pm$ 1.3%	-
P$_{range}$ [GeV]	3-33	5-100	0.5-6.5
purity	mixed beam	> 99%	mixed beam

For handling and stacking purposes, the modules were assembled on a strong-back in strip units of four modules in the vertical direction. In order to scan the entire surface of all four modules they were placed on a remotely
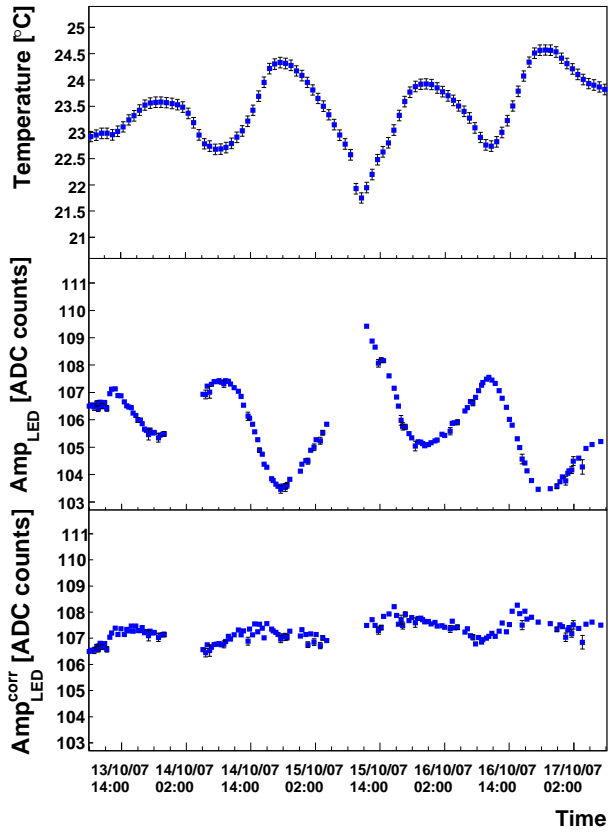
FIG. 1: Upper panel: temperature measurement as a function of time. Mid panel: LED signal amplitude for a typical tower for the same time interval. Lower panel: corrected LED signal amplitude.

controlled movable platform. The range of both horizontal and vertical adjustment allowed to scan the whole array of modules.

The EMCal readout electronics were attached to the back of the array of modules with the electronics cards and readout units located on the same moveable table as the modules, together with the low voltage supplies. In both setups at CERN and FNAL, a pair of scintillator paddles upstream of the EMCal was used for the beam definition trigger. In addition, at the CERN PS and at the FNAL MTEST, the signals from gas threshold Čerenkov counters were used as an electron trigger for electron/pion discrimination. A set of three MWPCs in front of the EMCal provided $x - y$ position measurements with better than 1 mm position resolution for the setup at FNAL. The MWPCs were used to define the beam particle trajectory which could then be projected to the front face of the EMCal modules.

The official ALICE data aquisition (DATE v6.13) [10] was used for taking the EMCal data. The MWPC data was recorded with a CamacCrate-via-USB (CCUSB) readout system. The data from the Čerenkov counters
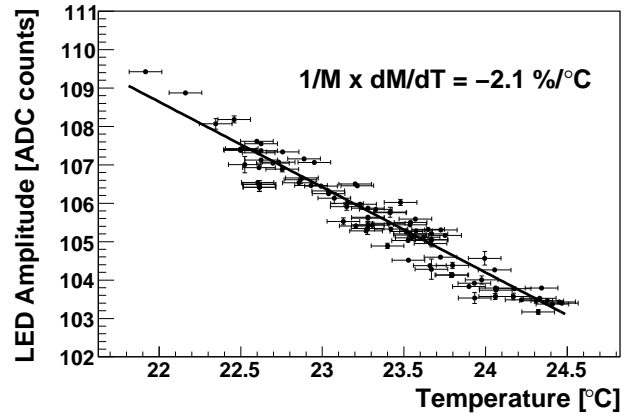

FIG. 2: LED signal amplitude as a function of the measured temperature.

were also recorded via the CCUSB system. The EMCal data were combined with the data from the trigger detectors and from the MWPCs offline, aligning the information from the different data streams spill-by-spill.

LED calibration system

In order to reach the design EMCal energy resolution for high energy electromagnetic showers, a tower-by-tower relative energy calibration of better than 1% has to be obtained and maintained in the offline analysis. In addition, since analog tower energy sums provide the basis of the level L0 and L1 high energy shower trigger input to the ALICE trigger decision, the EMCal should operate with APD gains adjusted to match online relative tower energy calibrations to better than 5%.

A LED calibration system, in which all towers view a calibrated pulsed LED light source, has been successfully tested to track and adjust for the temperature dependence of the APD gains during operation. The LED triggers were collected in parallel with the beam particle events throughout the entire CERN test beam measurements. These measurements were performed with the APDs operated at the nominal fixed M=30 gain.

The variation of the EMCal response to the LED signal with time and temperature was studied in order to test the system for calibration purposes. The temperature was monitored by a total of eight temperature sensors installed on the back surface of the module. The measured LED signal amplitude variation for a given tower as a function of time is compared in Fig. 1 for the same time interval with the temperature readings from the nearest sensor for the module in which the tower was located. A clear anti–correlation is observed.

Over the whole data taking period, some sharp vari-

ations in the LED signal amplitude were observed that cannot be attributed to temperature changes but rather to LED light yield changes, as when the setup was re-configured. These changes of the overall LED light were taken into account with an iterative extraction of the temperature coefficients. First, a new time interval was defined if an APD amplitude changed by more than 20 % from one hour to the next. For each time interval, both low and high gain LED signal amplitudes were fit simul-taneously as planes in space defined by signal amplitude, temperature, and the time interval. In a first iteration, all points deviating by more than $1.5\,\sigma$ from a predefined slope range $(0.015 < |\mathrm{d}M/\mathrm{d}T|\,[\%/^\circ\mathrm{C}] < 0.025)$ were ex-cluded. In the next iteration, the cleaned sample was fit with a free parameter for the slope in order to define the temperature coefficient. Fig. 2 shows the LED amplitude for a typical tower as a function of the temperature and for a certain time interval. The temperature coefficients obtained from the fits of these distributions were used to correct for the time dependence of the APD gain. As an example, the corrected LED amplitude is shown in the lower panel of Fig. 1 for the considered time interval.

The selected LED event amplitudes as well as the in-formation from the temperature sensors as a function of time are stored in a database. An interface was devel-oped and tested that allows for time-dependent calibra-tion corrections in the offline analysis of the test beam data.

Signal reconstruction

The digitized time samples from the read out have an amplitude as a function of time t that can be described with the form of a Γ-function in $ADC(t)$, where

$$ADC(t) = \text{pedestal} + A \cdot e^{-n} \cdot x^{\mathrm{n}} \cdot e^{\mathrm{n}\cdot(1-x)}\,, \qquad (1)$$
$$x = (t - t_0)/\tau\,.$$

Here, $\tau = \mathrm{n}\cdot\tau_0$ with the shaper constant τ_0 and n=2 as the shaper is gaussian of second order (composed of a dif-ferentiator and two integrators [9]). The charge collected from the APD, and hence the energy deposited in the tower, is proportional to the value of the parameter A at the time value $(t_0 + \tau)$ where the function peaks.

The test beam data were used to investigate the per-formance of this function and the parameters were opti-mized. The High-Low gain correlation was studied using the electron data in order to determine a threshold value for the amplitude for which the low gain rather than the high gain needs to be used due to saturation (at 1023 ADC counts). A good High-Low gain correlation with an average ratio of 16.3 between both gains was found up to 1050 ADC counts when using the values from a fit for ADC counts > 1000.

An overall inter-calibration procedure was carried out for all towers by normalizing the hadron MIP amplitudes
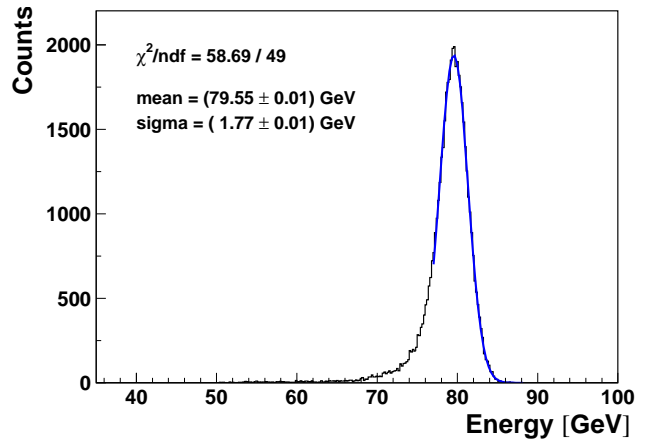

FIG. 3: Reconstructed energy for 80 GeV incident electrons. The curve represents a fit of a truncated gaussian to the his-togram with fit results as given in the figure.

in each tower, to a reference tower. Isolation of the MIP peak was achieved requiring, for each tower, no energy deposit in the surrounding eight towers. An alternative inter-calibration map was also considered by using the in-formation given by the electron beam peak in each tower. An absolute calibration for each tower was accomplished by comparing the nominal electron beam energy with the corresponding peak in the energy spectrum, as obtained by a sum over a 3×3 tower cluster. For this purpose, 3×3 local cluster inter-calibration coefficients were extracted from the overall map, by choosing each tower in turn as a reference. This allowed evaluation of the energy spec-trum by a sum over the 9 towers in the cluster, with a proper calibration adjusted to match that of the central tower in each cluster. These calibration coefficients were used to analyse the test beam data with the standard ALICE cluster reconstruction software. Fig. 3 shows the reconstructed energy for 80 GeV incident electrons (for a typical run).

Linearity and uniformity of energy response

The absolute energy calibration obtained by a sum over a 3×3 tower cluster is shown in Fig. 4. The lin-earity of the response is better than 1% over the full energy range down to 20 GeV. At low energies, thresh-old effects become non–negligible compared to the to-tal energy deposited and light transmission losses might have an impact. In fact, as shown in the bottom panel of Fig. 4 by the full circles the reconstructed energy is systematically lower than the incident one for energies equal or below 10 GeV. A drop of $\sim 10\%$ is observed at 5 GeV. This behaviour is well described by a cubic function as demonstrated by the open circles in Fig. 4 (bottom panel). At high energies, deviations of the ratio from unity are expected due to longitudinal shower leak-
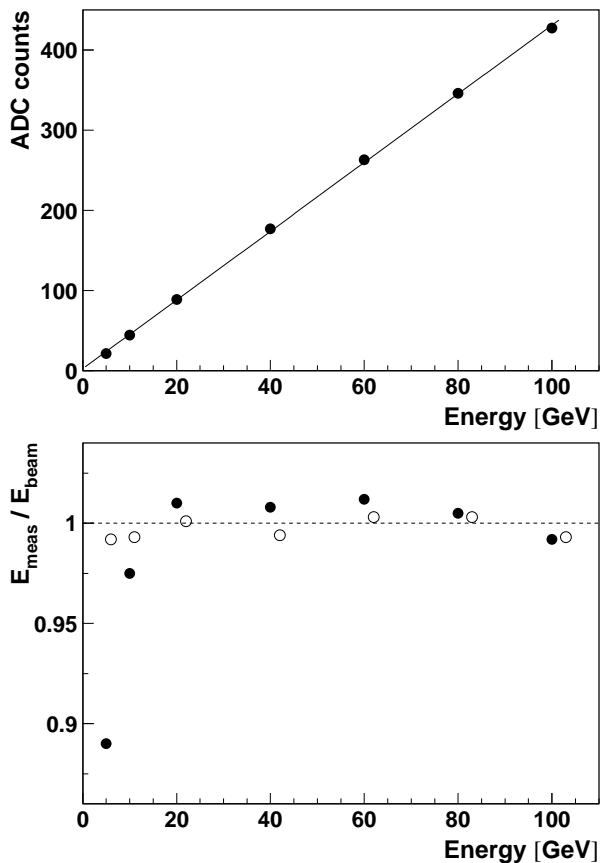
FIG. 4: Top: Linearity of the response for a sum over a 3×3 tower cluster as a function of the incident beam energy. The solid line is a linear fit to the data. Bottom: Ratios between the linear fit and the data (full circles) and a cubic fit and the data (open circles). The dashed line is placed at a ratio of unity to guide the eye.

age. The data show an indication of such an energy loss at high energies.

The uniformity of the energy response was studied for several different conditions. All module centers and a major part of tower centers were scanned using 80 GeV electrons. In addition, data were taken across tower and module borders. A uniformity of the energy response was found with a RMS better than 1 GeV, for 80 GeV incoming electrons. This result implies a very good uniformity of the response (within 1%) for the EMCal as constructed.

Light Yield

The light yield, the number of photoelectrons at the APD per unit of electromagnetic energy deposited in the EMCal (photoelectrons/MeV), determines the overall APD+shaper gain required to match the desired dynamic range in ALICE. Due to the large number of individual towers planned for the final design of the EMCal,

it is also important to estimate the tower-to-tower dispersion of the light yield.

During the test beam, the APDs were all operating at gain M=30. The individual voltage settings had been established for each APD prior to the test beam measurements. This procedure compares the amplitude at a given bias voltage to the amplitude measured at low voltages, where the gain is assumed to be unity [5]. The light yield (LY) at the gain M=30, for each individual tower, is then extracted following

$$LY(p.e./MeV) = (channels/MeV) \cdot (1/G_A) \quad (2)$$
$$\cdot (1/P_G) \cdot (1/ADC_{conv}),$$

where the shaper amplifier gain $G_A = 0.229$, the charge voltage conversion factor of the preamplifier $P_G = 0.83$ V/pC and the ADC conversion $ADC_{conv} = 1024$ channels/V. The light yield at unit gain (M=1) is obtained from this value divided by 30. An average light yield of about (4.3 ± 0.3) photoelectrons/MeV, was found, which is consistent with the light yield value of PHOS.

Energy resolution

The energy resolution of an electromagnetic calorimeter can be parameterized as

$$\sigma(E)/E = a \oplus b/\sqrt{E} \oplus c/E , \quad (3)$$

where E is the measured energy. The intrinsic resolution is characterized by the parameter b that arises from stochastic fluctuations due to intrinsic detector effects such as energy deposit, energy sampling, light collection efficiency, etc. The constant term, a, originates from systematic effects, such as shower leakage, detector nonuniformity or channel-by-channel calibration errors. The third term, c, is due to electronic noise summed over the towers of the cluster used to reconstruct the electromagnetic shower. The three resolution contributions add together in quadrature.

Detailed GEANT3 Monte Carlo simulations for the final module design yield fit results using Eqn.(3) of $a = (1.65\pm0.04)\%$, $b = (8.0\pm0.2)\%$ and $c = (7.4\pm0.2)\%$ over a photon energy range of 0.5 GeV to 200 GeV. These results are based on energy deposition only and do not include photon transport efficiencies. Systematic contributions to the resolution arising from calibration and related systematic uncertainties are ignored. The value of the constant term a is dominated by longitudinal shower leakage in these calculations. Other systematic effects, which arise during detector fabrication and from the tower-by-tower calibration uncertainties, will increase a.

By combining data taken at the CERN PS and SPS the calorimeter resolution over the energy range of 0.5 GeV
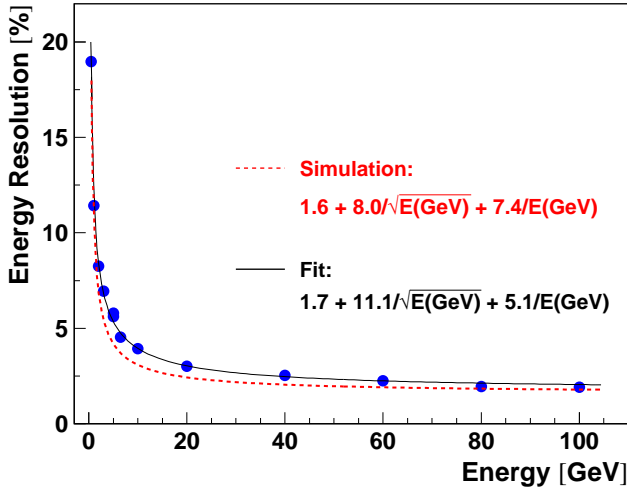
FIG. 5: Energy resolution for electrons as a function of the incident beam momentum. The beam energy spread was subtracted from the measured result. The dashed curve represents the resolution obtained from Monte Carlo simulations.
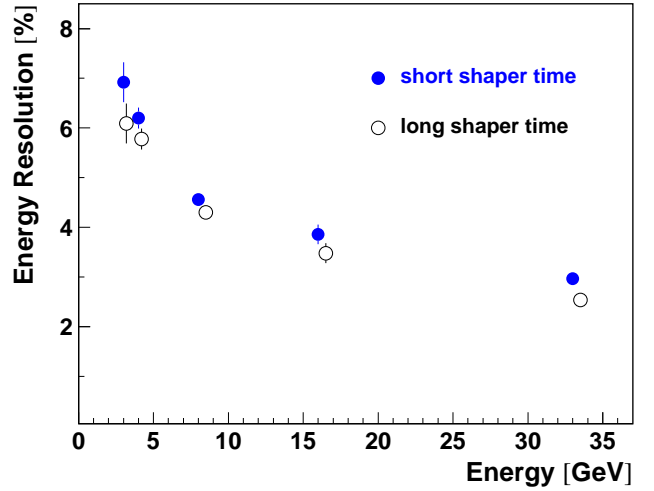

FIG. 6: Energy resolution for electrons as a function of the incident beam momentum for short (full circles) and long (open circles) shaper time, corresponding to the EMCal and PHOS design, respectively. The open circles are slightly shifted to the right for visibility.

to 100 GeV could be explored. Such energy scans were performed at several different positions, including tower and module edges. The LED calibration system was used to track and adjust for the time dependence of the calibration coefficients. No systematic variation of the resolution depending on the position was observed. The resolution obtained at the different positions was combined and the average values as a function of the incident beam momentum are displayed in Fig. 5. The momentum spread of the incident beam of typically 1.3% was subtracted in quadrature. A fit to the energy resolution as a function of the incident energy following Eqn.(3) is also shown in Fig. 5 with parameters $(a = 1.7 \pm 0.3)\%$, $(b = 11.1 \pm 0.4)\%$ and $(c = 5.1 \pm 0.3)\%$. These parameters can be compared with the GEANT3 simulation result for the EMCal module geometry described before and presented by the dashed line in Fig. 5. The increase of the stochastic term b, representing a worse intrinsic resolution compared to the Monte Carlo simulations, is mainly due to light attenuation and light collection inefficiencies which were not modelled. The small increase of the constant term a demonstrates a stable, high quality detector fabrication and a good tower-by-tower calibration. The linear term, modelling electronic noise contributions, is set too high in the simulation.

The energy resolution was also studied for different incidence locations corresponding to the modules as installed in ALICE. Most of the test beam data were taken with a configuration where the beam hits the EMCal modules perpendicularly, corresponding to $z = 0, \eta = 0$ position. Data were also taken with configurations where the modules were tilted in ϕ by 6 or 9 degrees at different surface positions. The energy resolution for such tilted configurations compares well with the average

resolution as a function of energy presented in Fig. 5. No significant deviations from the average resolution at zero degree was observed.

Using the data from the FNAL test beam, possible effects of the shorter design shaping time for the EMCal of 200 ns (compared to 2 μs for PHOS) were studied. Fig. 6 shows the energy resolution as a function of the incident energy. The results are shown separately for the short (full circles) and long (open circles) shaping time readout regions of the test setup, averaged over various runs in each region. The resolution slightly deteriorates when using the short shaping time but is still well within the detector requirements.

Position resolution

The segmentation of the calorimeter allows one to obtain the hit position from the energy distribution inside a cluster with an accuracy better than the tower size. The x and y coordinate locations are calculated using a logarithmic weighting [11] of the tower energy deposits. Data from the FNAL test beam were used where the MWPCs provided a reference position measurement of better than 1mm. Fig. 7 shows the x and y position resolution as a function of the energy deposit for electrons. As expected, no difference in the resolution in the x and y directions is observed. The electromagnetic shower position resolution is seen to be described as 1.5 mm $\oplus$ 5.3 mm/$\sqrt{E(\text{GeV})}$, where the two contributions add together in quadrature.
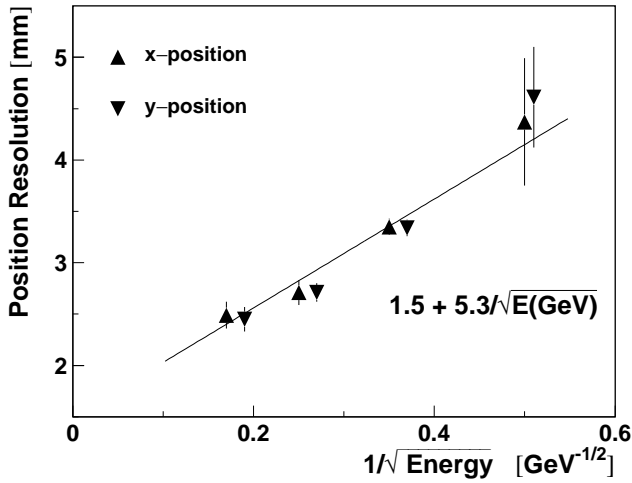
FIG. 7: Dependence of the position resolution as a function of the deposited energy for electrons. The curve shows the best fit result. The triangles representing the resolution for the y-position are slightly shifted to the right for visibility.

FIG. 8: EMCal response to hadrons (full histogram) and electrons (dashed histogram) of 100 GeV.

Response to hadrons

The EMCal can further enhance the ALICE particle identification capabilities due to the characteristically different response to electrons and hadrons. While electrons leave all their energy in the calorimeter, hadrons leave only a fraction of their energy but show a long tail due to hadronic showers. At the CERN PS pure electron and hadron beams were available. Fig. 8 shows the reconstructed energy for an electron and hadron beam of 100 GeV, which illustrates this very distinct response to electrons and hadrons. The high energy tail in the hadron response originates from processes such as charge exchange $\pi^- + p \rightarrow \pi^0 + n$, where most of the energy of the charged pions goes into neutral pions. These neutral pions decay immediately into photons starting a cascade which is indistinguishable from an electron–initiated shower.

The hadron rejection factor is defined as the number of all hadrons divided by the number of hadrons misidentified as electrons. This factor is shown in Fig. 9 as a function of the incident hadron beam energy for electron identification efficiencies of 90% and 95%. Error bars give the total uncertainty, which is dominated by the systematic uncertainty of the evaluation. Results from a Monte Carlo simulation are also shown for an electron identification efficiencies of 90%. For each incident beam energy, the electron identification efficiency was determined by integrating the reconstructed energy distribution of the pure electron beam (dashed histogram in Fig. 8) from the right-hand side till a cut value corresponding to the chosen efficiency.

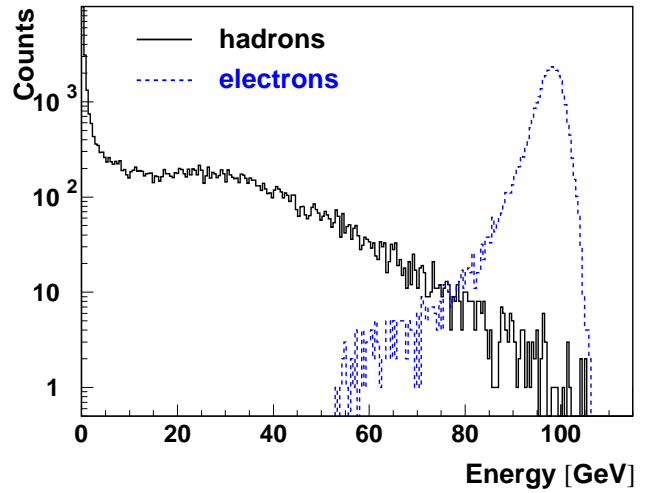A rejection factor of 10^2 to 10^3 is obtained over the energy range of 40 GeV to 100 GeV. Test beam data at
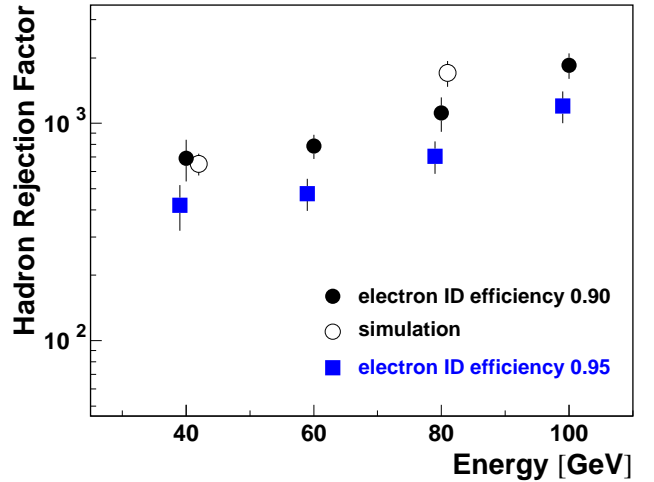

FIG. 9: Hadron rejection as a function of the incident hadron beam energy for an electron identification efficiency of 90% (circles) and 95% (squares). Error bars represent the total uncertainty. The open circles show the result from a Monte Carlo simulation for 90% electron identification efficiency. The squares (open circles) are shifted to the left (right) for visibility.

lower hadron energies were not taken. Hadron/electron rejection can be further improved by considering the characteristic shower shapes, as hadrons produce showers with wider spatial distributions than electrons.

Cosmic ray calibration

A calibration of all modules will be performed before their insertion in ALICE. The calibration procedure is based on a measurement of cosmic-ray muons at the minimum of ionization.

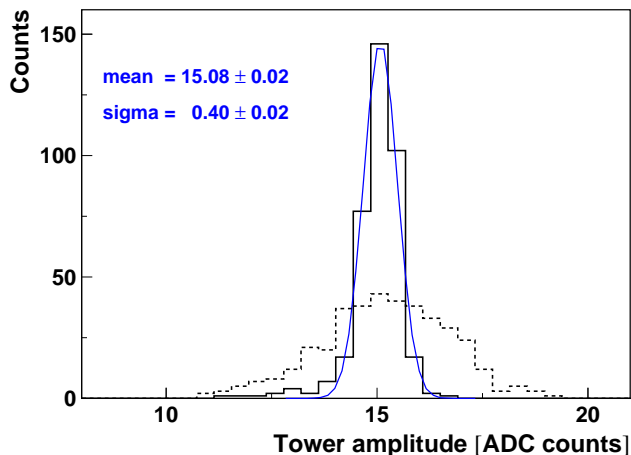The muon signal measured in each tower is obtained by

9

FIG. 10: Response of 384 towers of the EMCal to cosmic-ray muons before (dashed histogram) and after (full histogram) individual gain calibration. The curve represents a fit of a gaussian to the full histogram with fit results as given in the figure.

the use of an isolation procedure applied offline. For each event, the maximum signal amplitude is chosen and for all neighboring towers a signal smaller than a threshold value required. This threshold value is limited by the electronic noise (set to 3 ADC channels in the present case which amounts to about 15% of the muon energy).

Since the energy of MIP muons is too low to trigger the EMCal, an external trigger is necessary. The muons, passing the towers along their length, are selected using scintillator paddles. Each paddle covers 12 modules grouped into a 'strip module', and is read out at both extremities by photomultiplier tubes (PMT). This trigger configuration appeared to be the most reliable from the cosmic analysis test done in December 2007 [4] with the EMCal prototype described above. The time of flight difference between both PMTs allows one to select vertical muons with a spatial accuracy of a few centimeters. The isolation procedure then ensures that no energy was deposited in the neighboring towers. A 24-hour run allows the accumulation of about 500 muons per towers, which is sufficient to extract a MIP peak with an accuracy better than 1%.

An individual gain calibration is performed for each tower, so as to ensure that the amplitude of the average signal for cosmic muons is the same for all towers. The tower gains, which are controlled through the tower high voltage power, are tuned iteratively. Fig. 10 shows the dispersion of the mean amplitude of 384 towers before and after this procedure (thin and bold lines, respectively). After three iterations a final relative dispersion < 3% is reached.

CONCLUSION

The performance of a (4×4) array of prototype modules and of a (4×4) array of final design modules for the ALICE EMCal has been studied in test beam measurements at FNAL and CERN, respectively.
These studies demonstrate: (i) an average light yield of (4.3 ± 0.3) photoelectrons/MeV
(ii) an energy resolution of

$$\frac{\sigma(E)}{E}[\%] = (1.7 \pm 0.3) \oplus \frac{(11.1 \pm 0.4)}{\sqrt{E(\text{GeV})}} \oplus \frac{(5.1 \pm 0.7)}{E(\text{GeV})}$$

(iii) a uniformity of the response within 1% for all towers and configurations
(iv) a good linearity of the response to electrons in the energy range 10-100 GeV
(v) an only slightly deteriorated energy resolution when using the EMCal default shaping time of 200 ns compared to 2 μs for PHOS
(vi) a position resolution described by 1.5 mm $\oplus$ 5.3 mm$/\sqrt{E(\text{GeV})}$
(vii) a hadron rejection factor > 600 for an electron identification efficiency of 90%.

A LED calibration system was successfully tested to track and adjust for temperature dependent effects during operation.
Cosmic ray calibrations allow a precalibration of all modules prior to installation in ALICE with a relative spread of < 3%, sufficent for the use in an online trigger.
The performance of the tested EMCal modules reaches all design criteria.

ACKNOWLEDGMENTS

We gratefully acknowledge the CERN and the FNAL accelerator devisions for the good working conditions in the testbeam facilities. We would like to thank all engineers and technicians of the participating laboratories for their invaluable contribution to the construction of the EMCal. This work was supported by the Helsinki Institute of Physics and the Academy of Finnland; the French CNRS/IN2P3/INPG, the 'Region Pays de Loire', 'Region Alsace','Region Auvergne' and CEA, France; the Istituto Nazionale di Fisica Nucleare (INFN) of Italy; the Office of Nuclear Physics within the United States DOE Office of Science and the United States National Science Foundation.

[1] F. Carminati *et al.* (ALICE Collaboration), J. Phys. G30, 1517 (2004).

[2] ALICE Collaboration, Physics Performance Report, Vol 2, J. Phys. G (2006).

[3] ALICE Collaboration, K Aamodt *et. al.*, The ALICE experiment at the CERN LHC, JINST 3 (2008) S08002.

[4] ALICE Collaboration, ALICE Technical Design Report Electromagnetic Calorimeter, CERN-LHCC-2008-014, 1 December 2008.

[5] A. Badalá *et al.*, Prototype and mass production tests of avalanche photodiodes for the electromagnetic calorimeter in the ALICE experiment at LHC, Proceedings of NDIP08 Conference, Aix-Les-Bains (France) (2008), Nucl. Instrum. Meth. A 610 (2009) 200.

[6] The ALTRO chip: A 16-channel A/D converter and digital processor for gas detectors, Proceedings of IEEE NSS/MIC, Norfolk (USA), November 2002.

[7] Photon Spectrometer PHOS, ALICE Technical Design Report, CERN /LHCC 99-4, 5 1999.

[8] D.V. Aleksandrov *et. al.*, A high resolution electromagnetic calorimeter based on lead-tungstate crystals, Nucl. Instrum. Meth. A 550 (2005) 169.

[9] H. Muller *et. al.*, Configurable Electronics with Low Noise and 14-bit Dynamic Range for Photodiode-based Photon Detectors, Nucl. Instrum. and Meth. A 565 (2006) 768.

[10] ALICE DAQ, DATE V5 User's Guide, Internal Note ALICE-2005-015.

[11] T.C. Awes *et al.*, A Simple method of shower localization and identification in laterally segmented calorimeters, Nucl. Instrum. Meth. A 311 (1992) 130.